The origins of friction and the growth of graphene, investigated at the atomic scale

Baarle, D.W. van

Part II

Graphene growth on Ir(111)

Chapter 5

Introduction, instrumentation and methods

5.1 A short introduction to graphene

5.1.1 The need for reliable graphene production methods

After the experimental discovery of graphene by Geim et al. in 2004[33], this material has obtained enormous attention as many of the extraordinary properties that have been predicted theoretically, have been confirmed by scientific experiments. The uniqueness of graphene is in its internal structure. Graphene is the thinnest possible material, with a thickness of a single atom. It is a 2-dimensional network of carbon atoms solely, which are ordered in a honeycomb lattice. All carbon atoms are connected to each other via sp2-bonds, which make it mechanically the strongest material known. Although graphene sheets can be stacked, for example to form graphite, the VanderWaals interactions between the sheets are weak with respect to the strong, in-plane bonds.

The rather simple internal structure of graphene makes it attractive both theoretically and experimentally. For example, research has shown that graphene is resistant to many chemical environments, putting graphene forward as a candidate for protective coatings[34]. Its electronics properties make graphene promising for future electronics, for example for photonics, high-frequency and energy storage applications[35–37]. In addition to this, the strength and the 2-dimensional nature of graphene can be used to apply graphene on surfaces in order to reduce friction at interfaces[1].

For industrial applications and all other forms of large-scale use of graphene, e.g. in research, methods are required for mass production of high-quality graphene. The first samples of graphene were obtained via mechanical exfoliation of graphite[38]. Using Scotch tape, natural graphite was cleaved repeatedly until one layer of graphite (i.e. graphene) was left. This method is sufficient for many laboratory purposes, but does not satisfy industrial requirements of scalability and controlled quality. Currently, well-known ways to synthesize graphene applicable for mass production are the growth from silicon carbide (SiC) and the chemical vapor deposition (CVD) of graphene from a carbon containing gas on a transition metal[35].

It has turned out to be far from straightforward to synthesize graphene with a quality, e.g. defect density, as good as graphene obtained by mechanical exfoliation. Nevertheless, graphene production recipes are being developed delivering material of steadily improving quality[39, 40]. However, the graphene sheets produced nowadays still suffer from various issues, such as defects in the form of domain boundaries[41], contaminations and wrinkles that originate from the growth method or from used transfer methods[42, 43].

The most promising and and most widely used method to synthesize graphene is the growth via CVD. In this process, typically hydrocarbons are deposited on a transition metal. At a certain temperature, the hydrocarbon molecules decompose and leave carbon on the substrate. When appropriate conditions are applied (e.g. gas pressure, substrate temperature) the carbon atoms will form graphene nuclei and growth of graphene can be realized by further addition of carbon.

A complete understanding of the complex CVD-process is required in order to manage it such, that one can prevent the creation of defects and suppress other processes that degrade graphene. Once all stages of the graphene growth process are fully under control, a process flow can be designed such that nearly perfect, macroscopically sized layers of graphene can be synthesized. This should result in a reliable recipe to produce graphene on an industrial scale.

5.1.2 Graphene growth on Ir(111)

To study thin film growth, typically single crystals are used. The crystal surfaces are used as model systems and allow systematic research of the synthesis of e.g. graphene. A popular substrate surface used to grow graphene, is the Cu(111) surface. As the solubility of carbon in copper is relatively low, this substrate allows for self-limiting growth of monolayer graphene.

The growth of graphene on copper takes place at a temperature of approximately 1325 K. At this temperature, the vapor pressure of copper is so high, that copper is leaving the surface at a rate of approximately 200 monolayers per second[44]. This effect would make it hard to scan the surface with the STM for long periods of time as the surface level is retracting itself over time. In addition, we find that the scanning of a copper surface with the STM at 1325 K immediately leads to the formation of a 'neck' between the surface and the STM tip, like reported before in the case of scanning of Pb surfaces with an STM tip at a temperature of 318 K[45]. Summarizing, the growth of graphene on copper cannot be studied by STM *in situ* at the appropriate, high CVD temperaturef.

In order to use STM imaging to obtain atomic-scale insight in CVD growth of graphene on metal surfaces, we are forced to take refuge in alternative metals. One of the metal surface that we have employed for this purpose is Rh(111). Studies on this surface, performed in our research group, showed that the substantial solubility of carbon in rhodium cannot be neglected during growth of graphene[46]. Carbon that is dissolved into the rhodium bulk during the CVD process and that segregates to the surface of the rhodium crystal when the rhodium is cooled down to room temperature, subsequently, was found to affect the growth of graphene and to complicate the recipe to grow graphene with a minimal density of grain boundaries.

A metal that has both a low vapor pressure and a negligible carbon solubility is iridium. Ir(111) has been used already to study the growth of graphene, which revealed that the iridium surface is well suited for studying the growth of monolayer graphene in an ultrahigh vacuum (UHV) environment, even at high temperatures. Like several of the other metal surfaces, the lattice mismatch between Ir(111) and graphene leads to the formation of a superstructure, a moiré pattern, that enables one to study properties of graphene growth at the atomic scale, without necessarily having atomic resolution with the STM. For these reasons, Ir(111) was chosen as the substrate for our experiments.

The nucleation and growth of graphene on Ir(111) have been studied before using different techniques. Examples are: room-temperature investigation at the atomic scale by STM in UHV after temperature-programmed growth (TPG)[47]; real-time, *in situ* investigation by carbon evaporation in high vacuum by Low Energy Electron Microscopy (LEEM)[48] and real-time, *in situ* investigation of the thermal evolution of room-temperature deposited ethylene by high-energy-resolution, fast X-ray photoelectron spectroscopy[49]. These experimental approaches have improved significantly

the understanding of the growth mechanism of graphene on Ir(111). However, a direct observation of the nucleation, ripening and growth of graphene at the nanoscale is still lacking. A technique that would allow us to perform such observations might answer several fundamental questions on graphene synthesis.

A promising instrument to provide these nanoscale observations is the variable-temperature STM (VT-STM) in a UHV system[50]. This STM setup combines both the nanoscale resolution and the well-defined, variable- and high-temperature environment to study the nucleation and growth of graphene *in situ*. In our research group, such a microscope was developed and built-up several years ago. More details on this equipment can be found in the next section. In this part of the thesis, we present the experimental results on the graphene-iridium system, obtained using this home-built VT-STM.

5.2 Instrumentation

All experiments reported in this part of the thesis were performed in the UHV system that is described in more detail in the PhD thesis of M.J. Rost[51]. The system was located in the Huygens-Kamerlingh Onnes Laboratory of Leiden University. In this section we mention the most relevant components of this setup, with an emphasis on the parts that have been modified for the present work.

5.2.1 Vibration isolation

In order to reduce the influence of external vibrations, several measures were taken to minimize the sensitivity to these vibrations. First, the system is resting on a floor segment with separate foundation. Second, the vacuum system is put on four Newport[52] Laminar Flow Stabilizers. Next, the STM is suspended by a set of springs and finally an eddy current damping system is installed.

5.2.2 Vacuum system

The setup currently consists of four chambers, two of them containing a variable-temperature STM. These two chambers are connected to each other via a transfer chamber with a loadlock system attached to it.

The loadlock system

The loadlock system allows the users to load and unload both samples and STM scanheads/tips without venting the STM and transfer chambers. A Pfeiffer[53] TCM 180 magnetically levitated turbopump is used to pump down the loadlock compartment. Eurotherm[54] programmable temperature controllers and heating tapes are used to bake the loadlock system. In case a quick check or repair of either a sample or an STM scanner is needed, baking is not required: quick heating of the open loadlock unit in air using a heat gun, prior to pumpdown is sufficient.

The transfer chamber

The transfer chamber contains a mechanism to distribute samples or STM scanheads inside the whole vacuum system. This mechanism exists of a tape drive, which can be operated via two rotary feedthroughs. Using those feedthroughs, a tape with a carrier attached to its very end can be driven over a rails into the desired UHV chamber. Then, wobble sticks can be used to (un)load samples or scanners on the carrier. A Riber[55] ion pump is used to maintain the vacuum in the transfer chamber. Three pneumatic gate valves are located in between the transfer chamber and the other chambers (i.e. the loadlock system and the two STM chambers). Typically, the pressure in the transfer chamber is 1×10^{-8} mbar.

A new component added to the transfer chamber in the course of these studies, is a tip-sputtering system. This system consists of a Riber[55] sputter gun, which is used to sputter the STM tip with argon ions along the axial direction. A wobble stick is installed to pick up the STM scanner from the transfer system and to put it in front of the sputter gun. The sputter gun is aligned such that the 5 mm diameter ion beam hits the tip from the front. This method is used to clean the tip mildly, typically after experiments involving gas exposure.

The main STM chamber

The main chamber of the setup is equipped with a number of components that are listed in the PhD thesis of M.J. Rost[51]. Here, we list the most important components and those that have been added or modified during the work described in this thesis.

The base pressure of the chamber was most of the time below 1×10^{-11} mbar.

Turbomolecular pump A Pfeiffer[53] TCM 180 magnetically levitated 170 l/s pump is used to reach high vacuum and to pump during gas exposure. When high-resolution is aimed for, it is possible to turn off the pump without venting it.

Ion pump A 410 l/s Varian[56] Starr Cell ion pump is used especially for the low-pressure range and during high-temperature experiments.

Pressure Gauge The Varian[56] Bayard-Alpert Ion Gauge is now equipped with a UHV-24p, able to record pressures down to 7×10^{-12} mbar. The pressures listed in this thesis are not corrected for specific sensitivities to different gasses.

Sputter gun A differentially-pumped ion sputter gun from Specs[57] (IQE 12/38) is used in combination with a Wien filter to bombard the sample with 800 eV Ar^+ ions perpendicularly. The sputter gun is programmed to scan a square grid in order to optimally sputter the sample with a focussed beam. A typical sputter current measured through the sample was 220 nA.

As a transfer and loadlock system are used to exchange samples and STM scanheads, almost no reasons are left to vent the STM chamber. During the experimental work reported in this thesis, the STM chamber was vented and baked-out only once.

An additional, small STM chamber

A new vacuum chamber was added to the transfer chamber, which contains a second programmable temperature STM. It will contain only an STM, an ion sputter gun and an electron gun. The design of this chamber is kept very simple, which makes that this part of the system is expected to be even more stable and easier to use.

Gasses

The main source for the graphene synthesis in our experiments was ethylene gas. A 3.5 N purity high pressure gas bottle was purchased from Aldrich[58]. In order to grow the graphene by CVD, the substrate was exposed to ethylene via a leak valve.

Other gasses used for sputtering and annealing were 5.0 N Argon, 5.0 N Hydrogen and 5.0 N Oxygen bought from Messer[59] and packed in 1 L, 12 bar CANgas bottles.

5.2.3 The high- and variable-temperature STM

The STM that was used for the work reported here is the improved programmable temperature STM, which was also used by M.J. Rost, K. Schoots and G. Dong; its properties are discussed elsewhere, properties such as its high-temperature performance[50] and its high-speed capabilities[60]. This STM is situated in the largest vacuum chamber of the setup, which also has ion sputtering, mass spectrometry, Low Energy Electron Diffraction (LEED) and Auger electron spectroscopy facilities. Also, in this vacuum chamber, the sample can be exposed to precursor gasses, such as ethylene, in order to grow graphene by CVD. The uniqueness of the STM is its capability to allow the user to keep a specific area of the substrate in view during a substantial temperature variation of up to hundreds of Kelvin. In the work reported here, the STM was used in a temperature range from 298 to 1250 K. Typically, during an experiment, the STM was scanning the surface while the temperature was being increased. In this way, properties like the mobility and decomposition of deposits on the iridium substrate surface could be studied as a function of temperature.

An additional, special feature of the STM is its possibility to scan fast. This allowed us not only to scan at video rate (not used in the work reported here) but especially to realize high tip speeds and data rates. The core of this facility is in the analog scan generation combined with fast feedback control. We used a home-built pre-amplifier with a bandwidth of 50 kHz. All these components together allow the user to scan large areas at relatively high frame rates. For example, typically a $500 \times 500\,\mathrm{nm}^2$ surface area was scanned in 512×512 pixels in only 30 s.

The temperature of the substrate was measured via a K-type thermocouple that was welded directly to the surface using a laser spot welding technique. In this way, the true temperature of the substrate was measured and a systematic error in the temperature reading was minimized.

5.3 Methods

5.3.1 The substrate: Ir(111)

Although copper is the most popular substrate for large-scale production of graphene, in our work this material was not chosen. The main reason for this choice is that the vapor pressure of copper is too high: at a typical temperature for graphene synthesis (1325 K) copper atoms are leaving the substrate at a rate of approximately 200 monolayers per second[44]. This condition makes it impossible to scan at.

A good alternative is an iridium substrate. Like copper, it is a transition metal that catalyses the cracking of hydrocarbons into smaller components. Another property that both copper and iridium share is the low carbon solubility: this is a useful property for uniform monolayer growth of graphene layers. Unlike rhodium and ruthenium, no attention has to be paid to carbon segregation from the bulk e.g. when cooling down from graphene synthesis conditions[46, 61, 62]. Finally, the system graphene on iridium exhibits a superstructure that is visible at the nanometer scale. This so-called moiré pattern relaxes the requirement of atomic resolution. Atomic-scale defects in the graphene lattice are directly visible in the moiré pattern. More information on the moiré pattern is given further on in this chapter.

For the substrate, an Ir(111) crystal was purchased from Surface Preparation laboratory[63]. It had been aligned within 0.1° of the (111) orientation (using Laue and $\theta - 2\theta$ X-ray diffraction) and cut in the right shape to fit in our STM sample holder ($4.8 \times 4.8 \times 1\,\mathrm{mm}^3$). Finally, it was polished mechanically. Halfway the experimental period, the sample has been repolished due to thermocouple material that was found to be present on the crystal surface. This contamination was caused by an accidentally exposure of the sample to a very high temperature ($> 1300\,\mathrm{K}$) that allowed the thermocouple material to distribute itself partially over the iridium surface.

5.3.2 Sample preparation

The iridium single crystal was cleaned by cycles of argon sputtering, annealing in oxygen and hydrogen and finally flashing to high temperature in UHV. These steps will quickly be discussed here.

Argon ion sputtering was performed for about 50 min. This resulted in the removal of approximately 5 ML (assuming a sputter yield of 1). Sputtering was mainly used to remove surface contaminants and to damage graphene islands after a graphene-growth experiment. The latter is necessary in order to facilitate the removal of carbon during the oxygen and hydrogen treatments.

In case large amounts of carbon were expected to be present, the system was exposed to oxygen. However, iridium reacts with oxygen more strongly than e.g. rhodium. In the temperature range of $870 - 1000\,\mathrm{K}$, iridium is known to be converted to IrO_2(s) when oxygen is present[64–66]. Around 1370 K, the IrO_2 present on the surface will decompose or gaseous IrO_3 might form. This means that one should be careful when oxygen is brought into contact with iridium at high temperatures.

In our work, we exposed the surface to oxygen at room temperature

(typical exposure of 10 L), followed by a slow, 10-minute temperature ramp to 870 K in oxygen. In order to prevent the heating filament to break, the oxygen partial pressure was limited to 5×10^{-8} mbar during high temperature exposures.

The removal of residual hydrocarbons and oxides was performed by a hydrogen gas treatment after the oxygen exposure. This should result in the removal of both residual contaminants. We typically exposed our iridium sample to a 5×10^{-8} mbar partial pressure of hydrogen at a temperature of 1200 K for 10 min.

Each cleaning cycle was completed by a short (1 min) flashing of the sample to 1400 K in UHV. The pressure typically stayed below 1×10^{-9} mbar during this treatment. The high temperature was applied in order to remove residual oxide and argon that was implanted in the sample (see below). Additionally, the iridium surface was smoothened by the high-temperature step, resulting in wide terraces and clean, straight steps.

Before each experiment, the condition of the Ir(111) surface was checked by STM at room temperature. Special attention was paid to iridium terrace edges, as contaminants typically accumulate there and affect edge shapes. Cleaning was continued when contaminants and pinning sites were observed at the steps.

As a consequence of the normal-incidence bombardment of the surface with Ar^+ ions, a fraction of the argon can be implanted in the near-surface region. Indeed, sometimes residual subsurface argon was left after cleaning. This showed up in the STM images as local protrusions of the surface, as argon inclusions deformed the lattice[67]. The possible impact of the argon bubbles on our experiments was checked every time. Although the argon bubbles can act as nucleation sites, their density was sufficiently low ($< 1\,\text{bubble}/900\,\text{nm}^2$), that a significant influence on our analysis can be excluded.

5.3.3 Tip preparation

STM-tips were etched electrochemically from a 0.25 mm diameter tungsten wire. After etching, the tip was cleaned in an ultrasonic bath in acetone, ethanol and iso-propanol and then dried with nitrogen gas. In the loadlock system the scanner and the tip were baked out at a temperature of approximately 150 °C. Then the scanner was transferred from the loadlock chamber, via the transfer chamber to the STM chamber, where it was positioned over the sample, with the tip positioned over a corner of the sample with a few tens of micrometers distance in between tip and sample. In this configuration, the tip was cleaned in argon by a self-sputtering tech-

nique[68]. If desired, the tip was mildly cleaned by a head-on sputter gun, placed in the transfer chamber (see Section 5.2.2). This last step was typically applied after STM experiments involving exposure to hydrocarbons.

5.3.4 Imaging graphene on Ir(111) by an STM

In general, through the tunnelling current, the STM probes the local density of electronic states (LDOS) rather than a geometrical height of the features directly below the tip. As a consequence, the apparent height recorded by an STM in constant-current mode cannot be interpreted as a mere topography map of the surface in case the LDOS is not uniform over the imaged surface. The tunnelling properties and, hence, the imaging can also be affected strongly when the very end of tip apex has changed in composition, e.g. by a molecule that was picked up from the surface. In the current case of an iridium surface with carbon or graphene on it, the LDOS is indeed not uniform[69, 70]. Hence the apparent height and the contrast in the moiré structure are sensitive to the tunnelling voltage. Due to this effect, a direct interpretation of the images in terms of geometrical height contours would not be justified. In our work, the effects that might be caused by a differences in the LDOS or the tunnelling voltage are mentioned every time, in case they might influence our analysis. Typically, we have avoided to base our interpretation on absolute heights of the observed nanolayers measured in different experiments. For example, the interpretation of the analysis presented Figure 6.8 is based on the change of distribution of apparent heights of clusters imaged in one image, which is not dependent on the absolute heights of the observed clusters.

5.3.5 Interpretation of moiré patterns

The lattice mismatch between graphene and the Ir(111) surface results in a so-called moiré pattern[69]. These patterns, which typically have a lattice parameter of around 2.5 nm, have both a physical and a chemical origin due to the binding of graphene to the iridium substrate[70]. As a consequence, they are easily observable by STM. A major advantage of these patterns is that they provide us indirectly with atomic resolution on the graphene overlayer, also in cases where noise or poor tip quality would prevent true atomic resolution.

In our research group, work was done previously on the appearance of the moiré patterns by Dong[71]. As that work contained a minor, yet essential inconsistency in the labelling, a compact derivation of the moiré rotation angle and its lattice constant is given here for the case of graphene

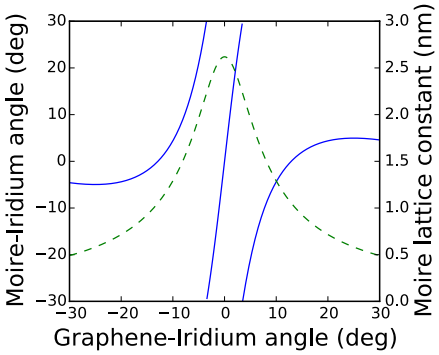

Figure 5.1: Two properties of the moiré pattern plotted as function of the angle between the graphene and iridium lattices. The solid, blue line represents the angle between the moiré pattern and the iridium substrate, calculated via Eq. 5.2. The dashed, green curve represents the lattice parameter of the moiré pattern, calculated via Eq. 5.3.

on Ir(111).

One of the primitive reciprocal lattice vectors of the moiré pattern, $\vec{k}_m$, can be computed directly from primitive reciprocal lattice vectors of both the graphene overlayer, $\vec{k}_{gr}$, and the iridium substrate, $\vec{k}_{ir}$:

$$\vec{k}_m = \vec{k}_{gr} - \vec{k}_{ir} \tag{5.1}$$

Using this construction, we can calculate several observables based on the geometrical situation. For this, we introduce the angle between graphene and iridium, α_{gr}, the angle between the moiré pattern and the iridium substrate, α_m and the lattice parameters of graphene, d_{gr}, iridium, d_{ir} and the moiré pattern, d_m. Following the derivation in the thesis of Dong, but now with correct labels, the angle between the iridium and the moiré pattern is obtained via

$$\alpha_m = \arcsin \frac{d_{gr} \sin \alpha_{gr}}{\sqrt{d_{gr}^2 + d_{ir}^2 - 2 d_{gr} d_{ir} \cos \alpha_{gr}}} \tag{5.2}$$

and the moiré lattice parameter is

$$d_m = \frac{d_{gr} d_{ir}}{\sqrt{d_{gr}^2 + d_{ir}^2 - 2 d_{gr} d_{ir} \cos \alpha_{gr}}}. \tag{5.3}$$

As the graphene-iridium system is six-fold symmetric, the parameters of the moiré pattern are fully described by plotting them as a function

of the graphene-iridium angle over an interval from $-30°$ to $30°$. The result is presented in Figure 5.1. An analogous treatment for the case of graphene on rhodium results in a qualitatively almost identical graph, with only minor quantitative differences due to the small difference in lattice constant between iridium and rhodium.